Relaxation time spectra of basaltic lavas between 500–1150 °C reveal patterns of Kramers–Kronig inconsistency of the complex viscoelastic shear modulus

Martin BEDNÁRIK*, Igor KOHÚT

Earth Science Institute of the Slovak Academy of Sciences, Division of Geophysics, Dúbravská cesta 9, P. O. Box 106, 840 05 Bratislava, Slovak Republic

Abstract: An important, yet until now neglected, aspect of the viscoelastic behaviour of lavas is the Kramers–Kronig consistency of their complex viscoelastic shear modulus. The most general linear viscoelastic model – the generalized Maxwell body with continuous relaxation time spectrum – produces a consistent storage and loss modulus, as can be verified by Kramers–Kronig formulae. We reprocessed the original datasets of the high-precision laboratory data by *James et al. (2004)* supplied as pairs of magnitude of the complex viscoelastic shear modulus and the loss angle. We introduce the magnitude-borne and loss-angle-borne logarithmic relaxation time spectra and their ratio as a suitable indicator of the linear viscoelastic inconsistency. The basaltic lavas from Etna, Hawai'i and Vesuvius have shown a general convergence to the ideal consistency with increasing temperature, although each sample with an individual inconsistency pattern. The biggest surprise is the inconsistency ratio rising to ∼20 in Etna 1992 top sample at 786 °C. Such a high inconsistency level still waits for an explanation and for the discoveries of its class-mates either in laboratory or field experiments.

Key words: viscoelasticity, generalized Maxwell body, Kramers–Kronig relationships, relaxation time spectrum, viscoelastic modulus inconsistency

1. Introduction

The basis for our curret work is provided by the study of *James et al. (2004)*. The amount and the quality of the laboratory viscoelastic data prompted us to reprocess it again, focusing on the phenomenon of viscoelastic inconsistency not addressed in the original study. We shall briefly summarize its

---

109

essence relevant to our study in the sequel.

The basaltic lava samples from Etna, Hawai'i and Vesuvius, heated up to temperatures between $\sim 500\,°C$ and $1150\,°C$ and fixed between Al rods of the apparatus (*Bagdassarov and Dingwell, 1993*), were subject to small forced harmonic torques ($\sim 10^{-3}\,N\,m$) generated by a synthesiser at frequencies between 0.002 and 20 Hz. The angular deformation across the sample was measured by pairs of capacitive pick-ups responding to the movement of pure iron plates located at the ends of the Al wings of the rods. The shear modulus and phase difference between the applied torque and the angular displacement were calculated from the phase and amplitude parameters of the sinusoids fitted to the recorded signals.

Two samples from Etna were collected from lava erupted in 1992. One of these samples was taken from the top surface, the other one from the base ($\sim 10\,cm$ down from the surface), and thus they represent samples with different cooling regimes. The surface sample has smaller vesicles (~ 0.2 to 0.5 mm, 15 to 20 vol. %) and smaller crystal content (~ 20 to 30 vol. %) than the basal sample (~ 20 vol. % of 1 to 2 mm vesicles and ~ 30 vol. % phenocrysts). No chemical composition of the samples was given either by the study itself, or by precedent studies. A further sample was collected from near the south east cone in 1999, from the least vesicular area found in a recently emplaced flow near hornito H3 (*Calvari and Pinkerton, 2002*) at the top of the active flow field. The sample was used to study mainly the crack-healing-related phenomena. The Etna 1999 sample data were not included in the dataset made available to us by the authors.

The Hawai'ian basalt was sampled in the east rift eruption zone of Kilauea from a lava flow from a pahoehoe toe in September, 1984 (eruption temperature $\sim 1147\,°C$). This pahoehoe lava flow corresponds to the episode 25 of the eruption Pu'u 'O'o of Kilauea Volcano. Its chemical composition has been presented in *Garcia et al. (1992)* and *Bagdassarov (2000)*. The vesicularity varies around 50 vol. %. The sample has ~ 10 vol. % of olivine quenched from magma during sampling and a few percent of other phenocrysts.

The Vesuvius samples were collected from the 1834 flow at Cava Ranieri approximately 6.3 km ESE of the central cone of Vesuvius by the group from University College of London. Chemical analysis of the samples is given in *Belkin et al. (1993)*. The same sample was also used by *Rocchi et al. (2004)*

110

in experiments to determine Young's modulus and tensile strength.

The most important findings of *James et al. (2004)* with respect to our study are the temporal variations in complex shear modulus and internal friction at $\sim 800\,^{\circ}$C. They suggest that, over durations of up to 120 hours, structural adjustments were occurring within some of the samples. This time-varying behaviour of lava samples is attributed to the slow closing (healing) of microcracks resulting in the apparent stiffening of lava samples under annealing. Thus, those parts of lava flows that underwent slow cooling have more elastic properties. Regions which cool faster possess smaller shear moduli and higher internal friction due to thermal microcracking.

Since the publication of *James et al. (2004)*, several other studies on rheological properties of lavas and other geomaterials were performed using the methods of mechanical spectroscopy (bending and torsional tests). We shall list here the ones addressing the factors that influence viscoelasticity at various time scales, temperatures and pressures: *Wagner (2004), Fontaine et al. (2005), Fontaine et al. (2008), Okumura et al. (2010), Takei et al. (2011), McCarthy et al. (2011), Chien (2014)* and *Okumura et al. (2016)*. Some of them could serve as a source of data for potential future viscoelastic consistency tests.

2. Consistency of viscoelastic storage and loss shear modulus according to Kramers–Kronig relationships

A causal and time-invariant linear system shall have a complex frequency response (FR) whose real and imaginary parts are consistent, i.e. complying with Kramers–Kronig relationships. Let us test whether the linear viscoelastic shear modulus represented by the generalized Maxwell body fits into this category.

The shear stress response $\tau(t)$ of the linear viscoelastic shear modulus of the generalized Maxwell body with finite number of Maxwell modes to the unit step in engineering shear strain:

$$\gamma(t) = \gamma\,\theta(t), \tag{1}$$

where γ is a constant and

$$\theta(t) = \begin{cases} 0 & \text{for } t < 0 \\ 1 & \text{for } t \geq 0 \end{cases},$$

is

$$\tau(t) = \begin{cases} 0 & \text{for } t < 0 \\ \gamma \sum_{n=0}^{N} g_n \exp\left(-t/\tau_n\right) & \text{for } t \geq 0 \end{cases}. \tag{2}$$

The Laplace transform of (1) and (2) yields $\gamma(s) = \gamma/s$ and $\tau(s) = \gamma \sum_{n=0}^{N} \dfrac{g_n \tau_n}{1 + s\tau_n}$, respectively. The shear modulus of the generalized Maxwell model then reads:

$$G(s) = \frac{\tau(s)}{\gamma(s)} = \gamma \sum_{n=0}^{N} \frac{g_n \tau_n}{1 + s\tau_n} \bigg/ (\gamma/s) = \sum_{n=0}^{N} \frac{g_n \tau_n \, s}{1 + s\tau_n}. \tag{3}$$

For a viscoelastic solid, one of relaxation times τ_n is infinite. Let us choose $\tau_0 \to \infty$. Then:

$$G(s) = g_0 + \sum_{n=1}^{N} \frac{g_n \tau_n \, s}{1 + s\tau_n}. \tag{4}$$

The substitution of $s = \mathrm{j}\omega$ yields the complex shear modulus:

$$G(\mathrm{j}\omega) = g_0 + \sum_{n=1}^{N} \frac{g_n \tau_n^2 \, \omega^2 + \mathrm{j} g_n \tau_n \omega}{1 + \tau_n^2 \omega^2} \tag{5}$$

denoted also as $G^*(\omega)$. The relaxed modulus G_R and unrelaxed modulus G_U are:

$$G_R = \lim_{\omega \to 0} G(\mathrm{j}\omega) = g_0, \quad G_U = \lim_{\omega \to \infty} G(\mathrm{j}\omega) = \sum_{n=0}^{N} g_n = G_R + \sum_{n=1}^{N} g_n. \tag{6}$$

The real part of (5) is the storage modulus:

$$G'(\omega) = g_0 + \sum_{n=1}^{N} \frac{g_n \tau_n^2 \, \omega^2}{1 + \tau_n^2 \omega^2}, \tag{7}$$

112

the imaginary part is the loss modulus:

$$G''(\omega) = \sum_{n=1}^{N} \frac{g_n \tau_n \omega}{1 + \tau_n^2 \omega^2} \,. \tag{8}$$

Let us verify that the storage (7) and loss modulus (8) satisfy the Kramers–Kronig relationships (*Kronig, 1926; Kramers, 1927*):

$$G'(\omega) = \lim_{\omega \to \infty} G'(\omega) - \frac{2}{\pi} \, \mathrm{PV} \int_0^\infty \frac{\omega' \, G''(\omega') - \omega \, G''(\omega)}{\omega'^2 - \omega^2} \, \mathrm{d}\omega' \,, \tag{9}$$

$$G''(\omega) = \frac{2\omega}{\pi} \, \mathrm{PV} \int_0^\infty \frac{G'(\omega') - G'(\omega)}{\omega'^2 - \omega^2} \, \mathrm{d}\omega' \,, \tag{10}$$

where PV denotes the Cauchy principal value of the integral.

Before we substitute (7) and (8) to (9) and (10), let us note that:

$$\mathrm{PV} \int_0^\infty \frac{\mathrm{d}\omega'}{\omega'^2 - \omega^2} = \lim_{\varepsilon \to 0^+} \left(\int_0^{\omega - \varepsilon} \frac{\mathrm{d}\omega'}{\omega'^2 - \omega^2} + \int_{\omega + \varepsilon}^\infty \frac{\mathrm{d}\omega'}{\omega'^2 - \omega^2} \right) = $$
$$= \lim_{\varepsilon \to 0^+} \left(-\frac{\mathrm{arctanh}((\omega - \varepsilon)/\omega)}{\omega} + \frac{\mathrm{arctanh}(\omega/(\omega + \varepsilon))}{\omega} \right) = 0 \,. \tag{11}$$

This means that in (9) and (10), any integrand with a constant numerator integrates to zero. The presence of the "null" terms (cf. e.g. *Rusu et al., 2005*) $-\dfrac{\omega \, G''(\omega)}{\omega'^2 - \omega^2}$ and $-\dfrac{G'(\omega)}{\omega'^2 - \omega^2}$ in (9) and (10), respectively, is a trick aimed at cancelling the singular term $\omega'^2 - \omega^2$ in the denominator of the integrand for suitably shaped $G'(\omega)$ and $G''(\omega)$, thus turning the integral from a singular into a non-singular one, as we shall see in the sequel.

The substitution of (7) and (8) to (9) yields:

$$G'(\omega) = g_0 + \lim_{\omega \to \infty} \sum_{n=1}^{N} \frac{g_n \tau_n^2 \omega^2}{1 + \tau_n^2 \omega^2} - \frac{2}{\pi} \sum_{n=1}^{N} \int_0^\infty \frac{g_n \tau_n}{1 + \tau_n^2 \omega'^2} \mathrm{d}\omega' = $$
$$= g_0 + \sum_{n=1}^{N} g_n - \frac{2}{\pi} \sum_{n=1}^{N} \frac{\pi \, g_n}{2 \, (1 + \tau_n^2 \omega^2)} = g_0 + \sum_{n=1}^{N} \frac{g_n \tau_n^2 \omega^2}{1 + \tau_n^2 \omega^2} \,, \tag{12}$$

113

which is the same as (7). Similarly, the substitution of (7) to (10) yields (omitting the term g_0 in (7) which integrates to 0 according to (11)):

$$G''(\omega) = \frac{2\omega}{\pi} \sum_{n=1}^{N} \int_0^\infty \frac{g_n \tau_n^2}{1 + \tau_n^2 \omega'^2} \mathrm{d}\omega' = \frac{2\omega}{\pi} \sum_{n=1}^{N} \frac{\pi \, g_n \tau_n}{2 \left(1 + \tau_n^2 \omega^2\right)} = \sum_{n=1}^{N} \frac{g_n \tau_n \omega}{1 + \tau_n^2 \omega^2}, \, (13)$$

which is the same as (8).

Thus, according to the Kramers–Kronig relationships, the storage and loss modulus of a viscoelastic solid with a finite number of Maxwell modes uniquely determine each other.

For $\tau_n > 0$, $G(s)$ is a minimum-phase function and $\ln G(s)$ is analytic for $Re(s) > 0$. Then the logarithm of the magnitude $\alpha(\omega) = \ln |G^*(\omega)|$ and the phase $\varphi(\omega)$ in $\ln G^*(\omega) = \alpha(\omega) + \mathrm{j}\varphi(\omega)$ form also a unique pair of functions (except for a constant term in $\alpha(\omega)$) coupled for instance by Bayard–Bode relationships (*Bode, 1945*):

$$\varphi(\omega) = \frac{1}{\pi} \int_{-\infty}^\infty \frac{\mathrm{d}\alpha(u)}{\mathrm{d}u} \, \ln \coth \frac{|u|}{2} \mathrm{d}u \tag{14}$$

and

$$\alpha(\omega) = \lim_{\omega \to 0} \alpha(\omega) - \frac{1}{\pi} \int_{-\infty}^\infty \frac{\mathrm{d}\left(\varphi(u)/\exp(u)\right)}{\mathrm{d}u} \, \ln \coth \frac{|u|}{2} \mathrm{d}u \tag{15}$$

or

$$\alpha(\omega) = \lim_{\omega \to \infty} \alpha(\omega) - \frac{1}{\pi} \int_{-\infty}^\infty \frac{\mathrm{d}\left(\varphi(u)\exp(u)\right)}{\mathrm{d}u} \, \ln \coth \frac{|u|}{2} \mathrm{d}u \,, \tag{16}$$

where $u = \ln\left(\omega'/\omega\right)$.

The reader can try to apply the formulae (14), (15) and (16) to $\alpha(\omega)$ and $\varphi(\omega)$ of a viscoelastic model with finite number of Maxwell modes only to discover that they fail to yield closed symbolic forms of the integrals. If we are not interested in asymptotic estimates, but in exact general transformations between $\alpha(\omega)$ and $\varphi(\omega)$ of a generalized Maxwell model with discrete

114

modes, the Bayard–Bode formulae are practically useless. In the next section, we shall offer alternative formulae practically applicable to generalized Maxwell body with both discrete and continuous relaxation spectrum and suitable for testing the consistency of $\alpha(\omega)$ and $\varphi(\omega)$.

3. Methods

3.1. Relaxation time spectra as consistency test tools

The formulae (7) and (8) could be used to extract the discrete spectra g_n, $n \in \{0, 1, \ldots, N\}$ for each of the sampled functions $G'(\omega)$, $G''(\omega)$ separately. The respective discrete spectra g'_n and g''_n could then be compared to assess the inconsistency of $G'(\omega)$ and $G''(\omega)$. The difficulty with the discrete spectra is the arbitrariness of both input sampling of $G'(\omega)$ and $G''(\omega)$ in frequency domain and output sampling of $g'_n(\tau_n)$ and $g''_n(\tau_n)$ in the domain of relaxation times, resulting in non-uniqueness and non-representativeness of the latter. Moreover, the formulae (7) and (8) do not have a form suitable for an effective numerical implementation of the inversion process, with a high potential of its failure.

We shall present a solution of this problem based on widely used continuous logarithmic relaxation spectra, comprehensively presented e.g. in *Ferry (1980)*. The shear stress response of a viscoelastic solid with continuous relaxation spectrum $H(\ln \tau)$ to unit step (1) is:

$$
\tau(t) = \begin{cases} 0 & \text{for } t < 0 \\ \gamma \left(g_0 \, \theta(t) + \int\limits_{-\infty}^{\infty} H(\ln \tau) \exp\left(-t/\tau\right) \mathrm{d}(\ln \tau) \right) & \text{for } t \geq 0 \end{cases} . \tag{17}
$$

After performing the Laplace transform, the shear modulus in the s-domain is:

$$
G(s) = g_0 + \int\limits_{-\infty}^{\infty} \frac{s \, \tau \, H(\ln \tau)}{1 + s \, \tau} \, \mathrm{d}(\ln \tau) \tag{18}
$$

and the storage and loss modulus are:

$$G'(\omega) = g_0 + \int\limits_{-\infty}^{\infty} \frac{\omega^2 \tau^2 H(\ln \tau)}{1 + \omega^2 \tau^2} \, \mathrm{d}(\ln \tau) \, , \tag{19}$$

$$G''(\omega) = \int\limits_{-\infty}^{\infty} \frac{\omega \tau H(\ln \tau)}{1 + \omega^2 \tau^2} \, \mathrm{d}(\ln \tau) \, . \tag{20}$$

Now it is natural to introduce the logarithmic frequency and relaxation time variables Ω, Θ (T cannot be used because it shall denote temperature). The substitution of $\tau = \exp(\Theta)$ and $\omega = \exp(\Omega)$ yields:

$$G'(\Omega) = g_0 + \int\limits_{-\infty}^{\infty} \frac{\exp(2\Omega + 2\Theta) \, H(\Theta)}{1 + \exp(2\Omega + 2\Theta)} \, \mathrm{d}\Theta \, , \tag{21}$$

$$G''(\Omega) = \int\limits_{-\infty}^{\infty} \frac{\exp(\Omega + \Theta) \, H(\Theta)}{1 + \exp(2\Omega + 2\Theta)} \, \mathrm{d}\Theta \, . \tag{22}$$

The kernel of the integral in (22):

$$K''(\Omega, \Theta) = \frac{\exp(\Omega + \Theta)}{1 + \exp(2\Omega + 2\Theta)} \tag{23}$$

is, for a fixed Θ, a bell-shaped function of Ω. The bell has its maximum at $\Omega_C = -\Theta$ and is exactly symmetric with respect to Ω_C. This bell shape is of utmost importance for the numerical implementation of the $G''(\Omega)$ to $H(\Theta)$ inversion. On the other hand, the kernel of the integral in (21)

$$K'(\Omega, \Theta) = \frac{\exp(2\Omega + 2\Theta)}{1 + \exp(2\Omega + 2\Theta)} \tag{24}$$

has an unpleasant form of a smoothened ramp growing from 0 to 1 as Ω goes from $-\infty$ to ∞.

The desired bell-shaped kernel appears in:

$$\begin{aligned}
\frac{\mathrm{d}G'(\Omega)}{\mathrm{d}\Omega} &= \int\limits_{-\infty}^{\infty} \frac{\mathrm{d}}{\mathrm{d}\Omega} \left(\frac{\exp(2\Omega + 2\Theta)}{1 + \exp(2\Omega + 2\Theta)} \right) H(\Theta) \mathrm{d}\Theta = \\
&= \int\limits_{-\infty}^{\infty} \frac{2 \exp(2\Omega + 2\Theta)}{(1 + \exp(2\Omega + 2\Theta))^2} \, H(\Theta) \mathrm{d}\Theta \, .
\end{aligned} \tag{25}$$

116

In this case, the kernel

$$\frac{\mathrm{d}K'(\Omega, \Theta)}{\mathrm{d}\Omega} = \frac{2\exp(2\Omega + 2\Theta)}{(1 + \exp(2\Omega + 2\Theta))^2} \tag{26}$$

forms a bell centred at $\Omega_C = -\Theta$ and exactly symmetric with respect to Ω_C. Compared to (23), the bell (26) is narrower.

The main idea of the $G''(\Omega)$ to $H(\Theta)$ and $\dfrac{\mathrm{d}G'(\Omega)}{\mathrm{d}\Omega}$ to $H(\Theta)$ inversion is based on the fact that due to the bell shape of the respective kernel, the value $H(\Theta)$ influences the functions $G''(\Omega)$, $\dfrac{\mathrm{d}G'(\Omega)}{\mathrm{d}\Omega}$ mainly at $\Omega = -\Theta$. The details will be provided in the section 3.2.

The experimental data from the harmonic measurements of the viscoelastic (shear) modulus are very often supplied in the form of samples of the magnitude of the complex modulus $|G^*(\omega)|$ and of the loss angle $\varphi(\omega)$. Both these datasets are likely to be contaminated by measurement errors characteristic to each of them. Computing $G'(\omega)$, $G''(\omega)$ out of $|G^*(\omega)|$, $\varphi(\omega)$ would produce an undesirable mixture of errors of $|G^*(\omega)|$ and $\varphi(\omega)$. An ideal approach to $|G^*(\omega)|$, $\varphi(\omega)$ is therefore their totally separate processing. We have realized that the Bayard–Bode relationships do not provide a reasonable option for the direct test of consistency of $|G^*(\omega)|$, $\varphi(\omega)$. We shall show that there is a viable alternative approach very similar to the use of relaxation time spectrum $H(\Theta)$ in (22) and (25).

Just for the purpose of a short derivation within this paragraph, let us consider the complex viscoelastic modulus $G_{01}^*(\omega)$ containing only the 0-th and the 1-st Maxwell mode. To avoid a variable confusion in the sequel, let us change g_0, g_1 to k_0, k_1 in advance. Then the modulus reads:

$$G_{01}^*(\omega) = k_0 + \frac{\omega^2\tau^2 k_1 + \mathrm{j}\omega\tau_1 k_1}{1 + \tau_1{}^2\omega^2}. \tag{27}$$

The tangent of its phase $\tan\varphi_{01}(\omega)$, where

$$\varphi_{01}(\omega) = \arctan\frac{\omega\tau_1 k_1/k_0}{1 + \omega^2\tau_1^2\left(1 + (k_1/k_0)\right)}, \tag{28}$$

has the same structure as the rational function $\dfrac{g_n\tau_n\omega}{1 + \tau_n^2\omega^2}$ – the summand of (8). Let us introduce $p_1 = k_1/k_0$ and compare the rational functions in (8) and (28) term by term: $g_n\tau_n = p_1\tau_1$, $\tau_n^2 = \tau_1^2\left(1 + p_1\right)$. Then

117

$$p_1 = \left(g_n^2 + g_n \sqrt{4 + g_n^2} \right) \Big/ 2 \tag{29}$$

and

$$\tau_1 = \tau_n \Big/ \sqrt{(1 + p_1)} \tag{30}$$

transform (28) to

$$\varphi_n(\omega) = \arctan \frac{g_n \tau_n \omega}{1 + \tau_n^2 \omega^2} \,, \tag{31}$$

which can be summed to the total phase

$$\varphi(\omega) = \sum_{n=1}^{N} \arctan \frac{g_n \tau_n \omega}{1 + \tau_n^2 \omega^2} \,. \tag{32}$$

Here, unlike in (8), g_n is dimensionless. Analogically to the transition from discrete (8) to continuous (20) representation, we can introduce a dimensionless relaxation time spectrum $h(\Theta)$ and write:

$$\varphi(\Omega) = \int\limits_{-\infty}^{\infty} \arctan \frac{\exp(\Omega + \Theta)\, h(\Theta)}{1 + \exp(2\Omega + 2\Theta)} \mathrm{d}\Theta \,. \tag{33}$$

We have to substitute (29) and (30) also to $G_{01}^*(\omega)$ in (27), denote $|G_n^*(\omega)| = |G_{01}^*(\mathrm{j}\omega)|$ and express it in terms of k_0, g_n and τ_n:

$$|G_n^*(\omega)| = k_0 \sqrt{1 + \frac{g_n^2}{2} + \frac{g_n}{2} \sqrt{4 + g_n^2}} \, \exp\!\left(\operatorname{arctanh} \frac{g_n \tanh(\ln \omega \tau_n)}{\sqrt{4 + g_n^2}} \right). \tag{34}$$

Alternatively, after the substitution of

$$p_2 = k_1 \Big/ (k_0 + k_1) = \left(-g_n^2 + g_n \sqrt{4 + g_n^2} \right) \Big/ 2 \,, \tag{35}$$

$$\tau_1 = \tau_n \Big/ \sqrt{(1 - p_2)} \,, \tag{36}$$

118

$$|G_n^*(\omega)| = (k_0 + k_1)\sqrt{1 + \frac{g_n^2}{2} - \frac{g_n}{2}\sqrt{4 + g_n^2}} \times$$
$$\times \exp\left(\operatorname{arctanh}\frac{g_n \tanh(\ln \omega \tau_n)}{\sqrt{4 + g_n^2}}\right). \tag{37}$$

Then the total magnitude of the shear modulus corresponding to the total phase $\varphi(\omega)$ (32) is:

$$|G_n^*(\omega)| = G_R \prod_{n=1}^{N} \sqrt{1 + \frac{g_n^2}{2} + \frac{g_n}{2}\sqrt{4 + g_n^2}} \times$$
$$\times \exp\left(\operatorname{arctanh}\frac{g_n \tanh(\ln \omega \tau_n)}{\sqrt{4 + g_n^2}}\right). \tag{38}$$

or

$$|G_n^*(\omega)| = G_U \prod_{n=1}^{N} \sqrt{1 + \frac{g_n^2}{2} - \frac{g_n}{2}\sqrt{4 + g_n^2}} \times$$
$$\times \exp\left(\operatorname{arctanh}\frac{g_n \tanh(\ln \omega \tau_n)}{\sqrt{4 + g_n^2}}\right). \tag{39}$$

In the case of continuous relaxation spectrum $h(\Theta)$ as in (33) (in the sequel, denoted as h for brevity), the integral forms corresponding to the latter two expressions are:

$$\ln|G_n^*(\Omega)| = \ln G_R + \frac{1}{2}\int_{-\infty}^{\infty} \ln\left(1 + \frac{h^2}{2} + \frac{h}{2}\sqrt{4 + h^2}\right) d\Theta +$$
$$+ \int_{-\infty}^{\infty} \operatorname{arctanh}\frac{h\tanh(\Omega + \Theta)}{\sqrt{4 + h^2}}\, d\Theta, \tag{40}$$

$$\ln|G_n^*(\Omega)| = \ln G_U + \frac{1}{2}\int_{-\infty}^{\infty} \ln\left(1 + \frac{h^2}{2} - \frac{h}{2}\sqrt{4 + h^2}\right) d\Theta +$$
$$+ \int_{-\infty}^{\infty} \operatorname{arctanh}\frac{h\tanh(\Omega + \Theta)}{\sqrt{4 + h^2}}\, d\Theta. \tag{41}$$

119

Similarly to the kernel $K'(\Omega, \Theta)$ in (24), also the integrand

$$K(\Omega, \Theta) = \operatorname{arctanh} \frac{h \tanh(\Omega + \Theta)}{\sqrt{4 + h^2}} \tag{42}$$

is a smooth ramp-like function of Ω. Therefore, for the purpose of $|G^*(\omega)|$ to $h(\Theta)$ inversion, we have to use the formula:

$$\frac{\mathrm{d} \ln |G^*(\Omega)|}{\mathrm{d}\Omega} = \int\limits_{-\infty}^{\infty} \frac{\mathrm{d}K(\Omega, \Theta)}{\mathrm{d}\Omega} \, \mathrm{d}\Theta = \int\limits_{-\infty}^{\infty} \frac{h \sqrt{4 + h^2}}{2 + h^2 + 2\cosh 2(\Omega + \Theta)} \, \mathrm{d}\Theta. \tag{43}$$

The integrand $\mathrm{d}K(\Omega, \Theta)/\mathrm{d}\Omega$ is a symmetric bell-shaped function of Ω centred at $-\Theta$. Once $h(\Theta)$ is known, it can be supplied back to (40) and (41) to yield G_R and G_U, respectively. The first terms in (40) and (41) are analogical to (9) in Kramers–Kronig or (15) and (16) in Bayard–Bode relationships, since $G_R = \lim\limits_{\omega \to 0} |G^*(\omega)|$, $G_U = \lim\limits_{\omega \to \infty} |G^*(\omega)|$ (cf. (6)). Note that G_R and G_U can be evaluated at any Ω. Their constancy over the frequency range indicates the quality of the inversion.

The quantity $h(\Theta)$ does not meet all usual expectations of a spectrum. The integral transformations (33) and (43) are (unlike (22)) non-separable into the classical spectral form $\int\limits_{-\infty}^{\infty} k(\Omega, \Theta)\, h(\Theta)\mathrm{d}\Theta$ and nonlinear in $h(\Theta)$. For our numerical implementation of the $h(\Theta)$ search, this is not a problem, as far as rough proportionality (the greater $h(\Theta)$, the greater $\varphi(-\Theta)$) is preserved. The phase $\varphi(\Omega)$ and the spectrum $h(\Theta)$ have roughly the same order of magnitude (cf. 52). For crustal rocks then $\varphi(\Omega) \to 0$, $h(\Theta) \to 0$. The reader can expand the functions used in the expressions (33) and (43) in Taylor series to see that for $h(\Theta) \to 0$ they converge to the usual integral transformation $\int\limits_{-\infty}^{\infty} k(\Omega, \Theta)\, h(\Theta)\mathrm{d}\Theta$.

In experimental practice, the formulae (22) and (25) give different $H(\Theta)$ spectra and the formulae (43) and (33) give different $h(\Theta)$ spectra. Therefore, we will speak of $G'(\omega)$-, $G''(\omega)$-, $|G^*(\omega)|$- and $\varphi(\omega)$-borne relaxation spectra and denote them accordingly: $H'(\Theta)$, $H''(\Theta)$, $h_{|G^*|}(\Theta)$ and $h_\varphi(\Theta)$. The method of *Winter (1997)*, giving a single discrete parsimonious spectrum for jointly inverted $G'(\omega)$, $G''(\omega)$ would be the less successful, the less $G'(\omega)$ and $G''(\omega)$ comply with Kramers–Kronig relationships.

120

With the introduction of the unscaled relaxation time spectrum $h(\Theta)$, we filled the grey field in the table of inversion schemes for viscoelastic consistency tests (Table 1).

Table 1. Inversion methods for viscoelastic consistency tests.

inversion	direct	via spectrum	
$G'(\omega) \leftrightarrow G''(\omega)$	Kramers–Kronig	standard	$G'(\omega) \leftrightarrow H(\Theta) \leftrightarrow G''(\omega)$
$\ln|G^*(\omega)| \leftrightarrow \varphi(\omega)$	Bayard–Bode	our solution	$\ln|G^*(\omega)| \leftrightarrow h(\Theta) \leftrightarrow \varphi(\omega)$

The measured and Kramers–Kronig inverted moduli $G'(\omega)$, $G''(\omega)$ are not as suitable consistency test tools as the relaxation time spectra $H(\Theta)$ or $h(\Theta)$ because of the ambiguity, which of $G'(\omega)$, $G''(\omega)$ shall be preferred as the comparison basis.

3.2. Numerical implementation of the consistency test based on the relaxation spectra

The numerical implementation of the spectral consistency test can be divided into three parts: data pre-processing, their inversion to spectra and the post-processing of spectra to retrieve additional characteristics (G_R, G_U, misfits of the spectra etc.). All the stages are implemented in a script in the computational environment Mathematica$^{®}$ by Wolfram Research.

We shall first describe the inversion itself, because it poses requirements to the input data to be met in the pre-processing stage. As an example, let us explain the inversion of $G''(\Omega)$ to $H(\Theta)$. The integral

$$G''(\Omega) = \int_{-\infty}^{\infty} \frac{\exp(\Omega + \Theta)\, H(\Theta)}{1 + \exp(2\Omega + 2\Theta)} d\Theta \quad (22)$$ shall first be discretized. The infinitesimal integration step $d\Theta$ shall be approximated by constant finite step $\Delta\Theta$ and the infinite integration range shall be approximated by finite range $\langle \Theta_{min}, \Theta_{max} \rangle$ such that $\langle -\Omega_{max}, -\Omega_{min} \rangle \subset \langle \Theta_{min}, \Theta_{max} \rangle$, where $\langle \Omega_{min}, \Omega_{max} \rangle$ is the frequency range of the $G''(\Omega)$ data. Typically, $\Theta_{min} \approx -2\,\Omega_{max}$, $\Theta_{max} \approx -2\,\Omega_{min}$. The original $G''(\Omega)$ must be extrapolated to the range $\Omega \in \langle -\Theta_{max}, -\Theta_{min} \rangle$.

The inversion shall be iterative according to the cyclic scheme:

121

$$G_i''(\Omega) = \sum_{n=1}^{N} \frac{\exp(\Omega + \Theta_n)\, H_{i-1}(\Theta_n)}{1 + \exp(2\Omega + 2\Theta_n)} \Delta\Theta \,, \tag{44}$$

$$c_i(\Theta_n) = G''(-\Theta_n) \Big/ G_i''(-\Theta_n) \,, \tag{45}$$

$$H_i(\Theta_n) = c_i(\Theta_n)\, H_{i-1}(\Theta_n) \,, \tag{46}$$

where i denotes the iteration number starting with $i = 1$. The $H_0(\Theta_n) = 1$ for all n can be used as start model. The ratio (45) of the original (inter- or extrapolated) data to their i-th synthetic approximation (44) gives the correction coefficients $c_i(\Theta_n)$ that will improve the estimate of $H_i(\Theta_n)$ (46). In (44), Mathematica allows us to use symbolic, continuous representation of $G_i''(\Omega)$.

With $G''(\Omega) \geq 0$ and $H_0(\Theta_n) > 0$, the repetition of (44÷46) can never arrive at $H_i(\Theta_n) < 0$. The correction coefficients themselves provide a suitable convergence criterion, as:

$$\lim_{i \to \infty} c_i(\Theta_n) = \begin{cases} 1 & \text{for } G''(-\Theta_n) > 0 \\[2mm] 0 & \text{for } G''(-\Theta_n) = 0 \end{cases} . \tag{47}$$

At $c_i(\Theta_n)$ approaching to either 1 or 0 for all n, the best possible approximation of $G_i''(\Omega)$ to $G''(\Omega)$ and $H_i(\Theta_n)$ to $H(\Theta_n)$ will be achieved within the bounds of the discretization and integration range truncation errors.

The convergence can be accelerated by a correction predictor more courageous than (45):

$$c_i(\Theta_n) = \left(G''(-\Theta_n) \Big/ G_i''(-\Theta_n) \right)^{\beta} \,, \tag{48}$$

where $\beta \in \langle 1, 2 \rangle$. As β approaches 2, the more uneven (oscillatory) the convergence is. At $\beta = 2$, the process diverges.

The schemes of inversion of other FRs to their respective time relaxation spectra are analogical to (44÷46).

The preprocessing should supply easily invertible data. We have to assure that $G''(\Omega) \geq 0$, $\dfrac{\mathrm{d}G''(\Omega)}{\mathrm{d}\Omega} \geq 0$, $\varphi(\Omega) \geq 0$, $\dfrac{\mathrm{d}\ln|G^*(\Omega)|}{\mathrm{d}\Omega} \geq 0$. It is usually not a problem with the first and third quantity in the list, but in $G'(\Omega)$,

122

$\ln |G^*(\Omega)|$ it often happens that on a part of their frequency range, they decrease with frequency. There, the negative values of $\dfrac{\mathrm{d}G'(\Omega)}{\mathrm{d}\Omega}$, $\dfrac{\mathrm{d}\ln|G^*(\Omega)|}{\mathrm{d}\Omega}$ shall be replaced by 0.

The truncation of the integration range is based on the assumptions $\lim\limits_{\Theta\to-\infty} H(\Theta) = 0$, $\lim\limits_{\Theta\to\infty} H(\Theta) = 0$, $\lim\limits_{\Theta\to-\infty} h(\Theta) = 0$, $\lim\limits_{\Theta\to\infty} h(\Theta) = 0$. If we want $H(\Theta)$, $h(\Theta)$ to go to zero already at $\Theta_{\min}$, $\Theta_{\max}$, we have to make sure that $G''(\Omega)$, $\dfrac{\mathrm{d}G'(\Omega)}{\mathrm{d}\Omega}$, $\varphi(\Omega)$, $\dfrac{\mathrm{d}\ln|G^*(\Omega)|}{\mathrm{d}\Omega}$ also go to zero at $\Omega = -\Theta_{\max}$, $\Omega = -\Theta_{\min}$. If it is not the case with the original (extrapolated) data, we have to apply band-pass filtering. A very abrupt transition from nonzero to (almost) zero values is not desirable, as it produces truncation artefacts in the relaxation spectrum. The filter must therefore offer a good trade-off between suppression in the stopband and smoothness around the cut-off frequencies.

We have very good experiences with the band-pass filter of the type:

$$F(\Omega - \Omega_0) = \left(1 + \sqrt{\left(\frac{\Omega - \Omega_0}{\Omega_{thr}}\right)^{2n}} \right)^{-1}, \tag{49}$$

where Ω_0 is the central frequency of the passband and Ω_{thr} is the cut-off frequency. $F(\Omega - \Omega_0)$ is an even function of $\Omega - \Omega_0$ even for an odd n, thus widening the set of candidates for its optimum order.

The lower are n and Ω_{thr}, the more the filter influences the data in the middle of the passband. As a consequence, the relaxation spectrum of the filtered FR may considerably differ from that of the original FR even in the passband. To minimize this effect, the original FR should be pre-deformed with the reciprocal band-stop filter and only then fitted by a polynomial of a suitably low order.

Let us denote the original data generally as $D(\Omega - \Omega_0)$. We have to produce the pre-deformed data:

$$D_{BS}(\Omega - \Omega_0) = D(\Omega - \Omega_0)\Big/F(\Omega - \Omega_0), \tag{50}$$

and fit it by the polynomial $P(\Omega - \Omega_0)$.

Then the optimal continuous representation of the original data within the passband of the filter is:

123

$$D_{BP}(\Omega - \Omega_0) = P(\Omega - \Omega_0)F(\Omega - \Omega_0)\,. \tag{51}$$

In the passband, the band-stop filter implicitly present in the pre-deformed data (50) cancels with the explicitly present band-pass filter in (51). In the stopbands, the band-pass filter prevails and suppresses the original FR. The main idea is very similar to that of pre-emphasis – de-emphasis signal processing.

When filtering $\ln|G^*(\Omega)|$, $G'(\Omega)$ or $\int\varphi(\Omega)$, $\int G''(\Omega)$, the order of the fitting polynomial $P(\Omega - \Omega_0)$ shall be equal to that of the filter (49). The desired band-pass filtering effect becomes obvious after the differentiation of the former quantities. In the stopbands, the values of derivatives will be negative and replaced by zero. If we accept a non-ideal stopband suppression, it is possible to fit $\varphi(\Omega)$ and $G''(\Omega)$ directly as well. The polynomials that fit them must then be of a lower order than the filter (49).

The lower n, the smoothest the transition from non-zero to zero values is and the smaller the cut-off artefacts in the corresponding spectra are.

Applying the same kind of filtering (51) to both sides of the couple subject to Kramers–Kronig relationships introduces their violation. This violation is however relevant only to the stopbands, where we do not expect to have any useful data.

A cleaner trick to suppress the stopbands is to subtract from the filtered FR a constant, whose equivalent in terms of constant ΔH or Δh we shall return to $H(\Theta)$ or $h(\Theta)$, respectively, at the very end. For instance, according to:

$$\Delta G'' = \int\limits_{-\infty}^{\infty} \frac{\exp(\Omega + \Theta)\,\Delta H}{1 + \exp(2\Omega + 2\Theta)}\,\mathrm{d}\Theta = \frac{\pi}{2}\,\Delta H\,, \tag{52}$$

a constant $\Delta G''$ subtracted from $G''(\Omega)$ shall be compensated by a constant $\Delta H = 2\Delta G''/\pi$ added to $H(\Theta)$. The negative values of thus lowered $G''(\Omega)$ are replaced by 0. This operation does not introduce any inconsistency with Kramers–Kronig relationships and is physically justified: a nonzero constant extrapolation of $H(\Theta)$ or $h(\Theta)$ to the zones not covered by data may be a more realistic estimate than their zero extrapolation. If we apply the same procedure to the linearized version of (33), we get $\Delta h = 2\Delta\varphi/\pi$. Similarly, we obtain also $\Delta H = \Delta\left(\mathrm{d}G'/\mathrm{d}\Omega\right)$, $\Delta h = \Delta\left(\mathrm{d}\ln|G^*(\Omega)|/\mathrm{d}\Omega\right)$.

124

One of the roles of the post-processing is to provide an independent check of the iteration outcome. Once $H(\Theta)$ is known, from (21) we yield $G_R = g_0$, which shall be constant over $\langle \Omega_{\min}, \Omega_{\max} \rangle$. For this purpose G_U can be used, as well. Its calculation requires G_R, though:

$$G_U = \lim_{\Omega \to \infty} G'(\Omega) = G_R + \int\limits_{-\infty}^{\infty} H(\Theta)\, \mathrm{d}\Theta\,. \tag{53}$$

Once $h(\Theta)$ is known, the formulae (40) and (41) can be used to obtain G_R and G_U, respectively. G_R and G_U and can be used as indicators of the consistency, as well. For this purpose, the spectra couples shall be obtained by compatible procedures, resulting in their nearly equal range of non-zero values.

An important part of the post-processing is the presentation of the results. The ratios $H'(\Theta)/H''(\Theta)$ and $h_{|G^*|}(\Theta)/h_{\varphi}(\Theta)$ or their reciprocals are particularly suitable for the inconsistency assessment provided the division by zero is avoided either by the subtract-return pre-processing or some other suitable means.

4. Results

The $h_{|G^*|}(\Theta)/h_{\varphi}(\Theta)$ ratios of the samples Etna 1992 top, Etna 1992 base, Hawai'i and Vesuvius are presented in Fig. 1 to 4. They are almost identical with the respective $H'(\Theta)/H''(\Theta)$ ratios. Therefore, the latter will not be presented here. The feature common to all samples is the convergence of $h_{|G^*|}(\Theta)/h_{\varphi}(\Theta)$ to 1 (ideal linear viscoelasticity) with the temperature increasing to the melting point.

At 500–600 °C, the scatter of the measured FRs allows for a large arbitrariness of their fits. Thus, the evidence for the convergence to ideal linear anelasticity with the temperature decrease is rather weak, but still visible in the case of Etna 1992 top. The biggest surprise is the very large $h_{|G^*|}(\Theta)/h_{\varphi}(\Theta)$ ratio (almost 20) of the Etna 1992 top sample at 786 °C. The measured $|G^*(\omega)|$, $\varphi(\omega)$ at 786 °C are very smooth and raise no doubts about their reliability. The batman-shaped transitions in $h_{|G^*|}(\Theta)/h_{\varphi}(\Theta)$ are due to the band-pass filtering of $\ln|G^*(\Omega)|$ and narrow kernel in (43).
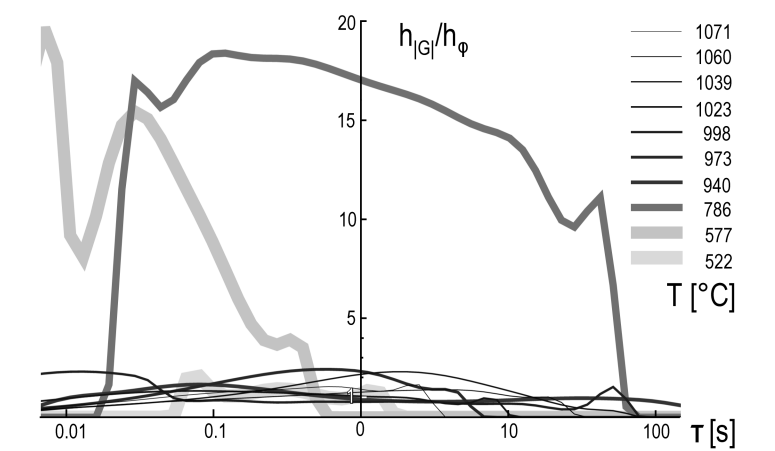
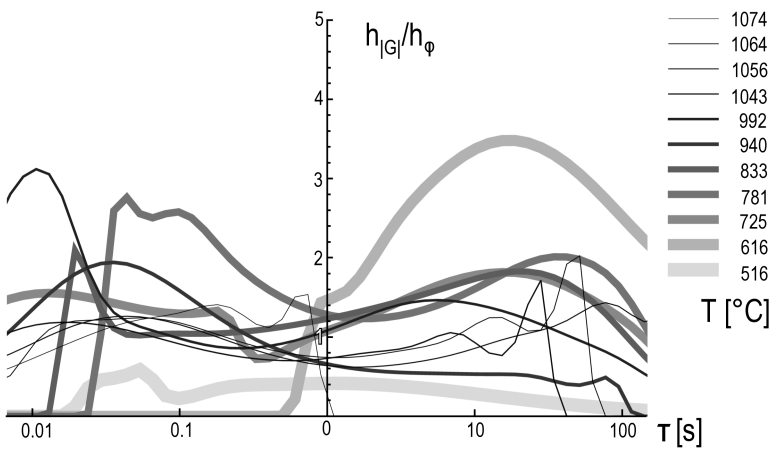Fig. 1. Linear viscoelastic consistency of the Etna 1992 top sample.

Fig. 2. Linear viscoelastic consistency of the Etna 1992 base sample.

The effects of $\varphi(\Omega)$ filtering on $h_\varphi(\Theta)$ are broader transitions without ringing, because the kernel in (33) is broader than in (43). Still, the filtering artefact is rather local and does not contaminate the whole spectrum. For the purpose of independent spectrum retrieval by the reader, we attached the source data of the Etna 1992 top sample in the Appendix (Table 2).

Similar, but not that pronounced inconsistencies can be seen in the samples Etna 1992 base ($h_{|G^*|}(\Theta)/h_\varphi(\Theta) \to 4$ already at 616 °C) and Hawai'i
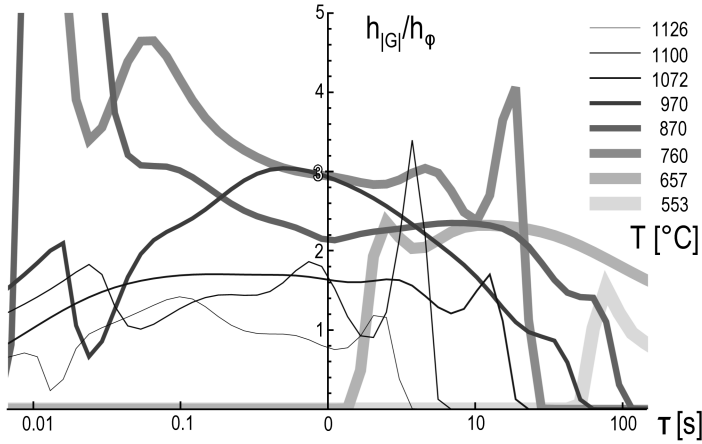
126

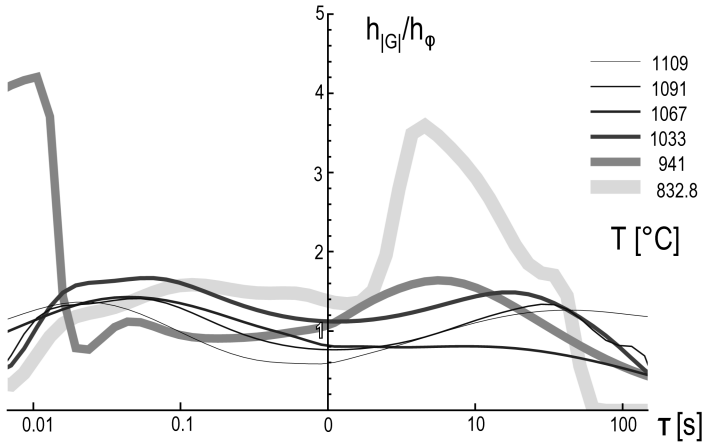Fig. 3. Linear viscoelastic consistency of the Hawai'i sample.

Fig. 4. Linear viscoelastic consistency of the Vesuvius sample.

$(h_{|G^*|}(\Theta)/h_\varphi(\Theta) \to 3$ at $760\,^\circ$C and $870\,^\circ$C). In the case of Vesuvius, the peak $h_{|G^*|}(\sim 4\,\mathrm{s})/h_\varphi(\sim 4\,\mathrm{s}) \to 4$ at $832.8\,^\circ$C (Fig. 4) is an artefact due to a sudden drop of $h_\varphi(\Theta)$ to the Δh_φ baseline, while $h_{|G^*|}(\Theta)$ continues its smooth run.

While the transition of the samples Etna 1992 and Vesuvius to the full consistency comes rather suddenly above $\sim 900\,^\circ$C, the Hawai'i sample shows a more smooth decrease to $h_{|G^*|}(\Theta)/h_\varphi(\Theta) = 1$. The curiosity of

127

the Hawai'i dataset at $553\,^{\circ}\mathrm{C}$ is $|G^*(\omega)|$ decreasing with frequency almost on the whole range of ω. Such behaviour is totally incompatible with the generalized Maxwell model. Therefore, we have a flat zero line of $h_{|G^*|}(\Theta)/h_\varphi(\Theta)$ at $553\,^{\circ}\mathrm{C}$ in Fig. 3. At lower temperatures, the decrease of $|G^*(\omega)|$ happens occasionally also in other samples and causes $h_{|G^*|}(\Theta)/h_\varphi(\Theta)$ to drop to zero. In Fig. 3 we also see the gradual retreat of the curves from lower frequencies with increasing temperature. This is due to an experimental fact mentioned by *James et al. (2004)* – at lower frequencies, the sample started to flow.

The best consistency is shown by the Vesuvius sample, owing also to the fact that the measurements start there only as high as at $832.8\,^{\circ}\mathrm{C}$.

5. Discussion

The unexpected discovery of viscoelastic inconsistency as large as 20 in terms of $h_{|G^*|}(\Theta)/h_\varphi(\Theta)$ ratio in Etna 1992 top sample demonstrates the importance of prompt consistency screening of any data deemed to be generated by a linear system. An early discovery by the authors themselves would have incited a thorough search for a possible error. With the error ruled out, one could concentrate on physics behind that strange behaviour. Now we are left with measurements of a single sample at a single temperature $786\,^{\circ}\mathrm{C}$ with neighbours as much as $200\,^{\circ}\mathrm{C}$ afar. The measurement with the original sample is unrepeatable, because in the course of being heated up to $1100\,^{\circ}\mathrm{C}$, the sample was completely annealed and lost its original material structure. Our experience with the rest of the dataset prepared by the authors who are specialists in this kind of measurements makes the probability of a huge error quite low and the matter is thus worth discussing it further.

The chemical and crystalline composition, although not stated, is roughly the same as in Etna 1992 base sample. The latter does not show any exceptional behaviour at $781\,^{\circ}\mathrm{C}$ (Fig. 2). Thus, a sudden crystal phase change cannot be blamed for the inconsistency. The authors of the original study identified the mechanism of crack healing as a possible cause of quality factor and shear modulus increase during the annealing. Due to the more intensive cooling of the surface of the lava flow, the Etna 1992 top sample exhibited more thermally-induced microcracking than Etna 1992 base. It is possible

128

that at $786\,^\circ\mathrm{C}$, the measurements are covering a non-equilibrium state in the middle of the crack healing process: the transformation of cracks into elliptical/spherical pores already decreased the loss angle, but the migration of volatiles out of the material and the decrease of the pore volume leading to shear factor increase is still in progress or waiting for higher temperatures. The high frequency torsions might propel the migration of volatiles more intensively than the low frequencies. Such extra stiffening with increasing frequency can add to the classical linear stiffening effect and increase $h_{|G^*|}(\Theta)$.

An alternative explanation is that even in an equilibrium multicomponent/multiphase system, especially at the possible onset of an additional relaxation mechanism (diffusion creep), one component can prevailingly influence the loss factor, the other the magnitude of the shear modulus. There can also be complicated nonlinear interactions between the components.

6. Conclusions

The main achievements of our current work are:

a) The introduction of $|G^*(\omega)|$-borne and $\varphi(\omega)$-borne relaxation time spectra, $h_{|G^*|}(\Theta)$ and $h_\varphi(\Theta)$, makes a totally separate treatment of the original $|G^*(\omega)|$, $\varphi(\omega)$ datastreams possible. The naturally unscaled spectra $h_{|G^*|}(\Theta)$, $h_\varphi(\Theta)$ are very well suited for comparing the attenuation of materials with very different scales of viscoelastic moduli. As an alternative to $h_{|G^*|}(\Theta)/h_\varphi(\Theta)$, the ratio $H'(\Theta)/H''(\Theta)$ can be used as viscoelastic consistency indicator and yields very similar results. The only serious methodological disadvantage of the latter approach is the mixing of the original $|G^*(\omega)|$, $\varphi(\omega)$ frequency responses and their errors.

b) Our method of iterative inversion of the frequency responses to relaxation time spectra is very stable, provided that the FRs are suitably prefiltered. The quality of the inversion can be checked by the calculation of the relaxed or unrelaxed shear modulus G_R, G_U. Ideally, they should be independent of Ω.

c) With temperature increase from $500\,^\circ\mathrm{C}$ to $1100\,^\circ\mathrm{C}$, the viscoelastic consistency of all examined lava samples improves to the ideal linear viscoelasticity. Nevertheless, each sample has a specific fingerprint. In the

Etna 1992 samples, there is a not very convincing evidence for fairly good consistency at $\sim 500\,°C$, then there is a loss of consistency between $\sim 600\,°C$ and $\sim 800\,°C$, especially dramatic in Etna 1992 top sample at $786\,°C$, where $h_{|G^*|}(\Theta)/h_\varphi(\Theta)$ approaches 20. This inconsistency level remains a mystery and a very strong motivation for a further search for extreme inconsistencies. If zones with that high inconsistency really occur within the lithosphere, then there could be a chance to detect them by seismic tomography.

References

Bagdassarov N. S., Dingwell D. B., 1993: Frequency dependent rheology of vesicular rhyolite. J. Geophys. Res., **98**, B4, 6477–6487, `doi: 10.1029/92JB02690`.

Bagdassarov N. S., 2000: Anelastic and viscoelastic behaviour of partially molten rocks and lavas. In: Bagdassarov N. S., Laporte D., Thompson A. (Eds.): Physics and chemistry of partially molten rocks. Kluwer, Dordrecht, pp. 29–66, `doi: 10.1007/978-94-011-4016-4_2`.

Belkin H. E., Kilburn C. R. J., De Vivo B., 1993: Sampling and major element chemistry of the recent (A.D. 1631–1944) Vesuvius activity. J. Volcanol. Geotherm. Res., **58**, 1-4, 273–290, `doi: 10.1016/0377-0273(93)90113-6`.

Bode H. W., 1945: Network Analysis and Feedback Amplifier Design. D. Van Nostrand, New York, 1945.

Calvari S., Pinkerton H., 2002: Instabilities in the summit region of Mount Etna during the 1999 eruption. Bull. Volcanol., **63**, 8, 526–535, `doi: 10.1007/s004450100171`.

Chien S.-Y., 2014: Rheological and Seismic Properties of Solid-Melt Systems: A Mechanical Spectroscopy Study. Springer Theses, `doi: 10.1007/978-3-319-03098-2`.

Ferry J. D., 1980: Viscoelastic Properties of Polymers, 3rd ed. John Wiley & Sons: New York.

Fontaine F. R., Ildefonse B., Bagdassarov N., 2005: Temperature dependence of shear wave attenuation in partially molten gabbronorite at seismic frequencies. Geophys. J. Int., **163**, 3, 1025–1038, `doi: 10.1111/j.1365-246X.2005.02767.x`.

130

Fontaine F. R., Ildefonse B., Neuville D. R., Mainprice D., 2008: Influence of viscosity variation of basaltic and andesitic melts on seismic attenuation in partially molten gabbronorite. Phys. Earth Planet. Inter., **167**, 3-4, 223–229, `doi: 10.1016/j.pepi.2008.04.010`.

Garcia M. O., Rhodes J. M., Ho R., Ulrich G., Wolfe E., 1992: Petrology of lavas from episodes 2-47 of the Puu OO eruption of Kilauea Volcano, Hawaii: evaluation of magmatic processes. Bull. Volcanol., **55**, 1-2. 1–16, `doi: 10.1007/BF00301115`.

James M. R., Bagdassarov N., Müller K., Pinkerton H., 2004: Viscoelastic behaviour of basaltic lavas. J. Volcanol. Geotherm. Res., **132**, 2-3, 99–113, `doi: 10.1016/S0377-0273(03)00340-8`.

Kramers H. A., 1927: The diffusion of light by atoms (La diffusion de la lumière par les atomes). Atti Cong. Intern. Fisica, (Transactions of Volta Centenary Congress) Como 2, 545–557 (in French).

Kronig R. d. L., 1926: On the theory of the dispersion of X-rays. J. Opt. Soc. Am., **12**, 6, 547–557, `doi: 10.1364/JOSA.12.000547`.

McCarthy C., Takei Y., Hiraga T., 2011: Experimental study of attenuation and dispersion over a broad frequency range: 2. The universal scaling of polycrystalline materials. J. Geophys. Res., **116**, B09207, `doi: 10.1029/2011JB008384`.

Okumura S., Nakamura M., Nakano T., Uesugi K., Tsuchiyama A., 2010: Shear deformation experiments on vesicular rhyolite: Implications for brittle fracturing, degassing, and compaction of magmas in volcanic conduits. J. Geophys. Res. Solid Earth, **115**, B6, `doi: 10.1029/2009JB006904`.

Okumura S., Kushnir A. R. L., Martel C., Champallier R., Thibault Q., Takeuchi S., 2016: Rheology of crystal-bearing natural magmas: Torsional deformation experiments at 800 °C and 100 MPa. J. Volcanol. Geotherm. Res., **328**, 237–246, `doi: 10.1016/j.jvolgeores.2016.11.009`.

Rocchi V., Sammonds P., Kilburn C. R. J., 2004: Fracturing of Etnean and Vesuvian rocks at high temperatures and low pressures. J. Volcanol. Geotherm. Res., **132**, 2-3, 137–157, `doi: 10.1016/S0377-0273(03)00342-1`.

Rusu C., Kuosmanen P., Astola J., 2005: Hilbert transform of discrete data: a brief review. In: Astola J., Egiazarian K., Saramäki T. (Eds.): Proceedings of The 2005 International TICSP Workshop on Spectral Methods and Multirate Signal Processing. SMMSP 2005, Riga, Latvia, 20–22 June 2005, pp. 79–84.

Takei Y., Fujisawa K., McCarthy C., 2011: Experimental study of attenuation and dispersion over a broad frequency range: 1. The apparatus. J. Geophys. Res., **116**, B09204, `doi: 10.1029/2011JB008382`.

Wagner N., 2004: Mechanical Spectroscopy on Volcanic Glasses. Dissertation (in German), FSU-Jena. Online, accessed 6 August 2018, available from: `http://www.db-thueringen.de/servlets/DerivateServlet/Derivate-2594`.

Winter H. H., 1997: Analysis of dynamic mechanical data: Inversion into a relaxation time spectrum and consistency check. J. Nonnewton. Fluid Mech., **68**, 2-3, 225–239, `doi: 10.1016/S0377-0257(96)01512-1`.

Appendix

Table 2. The frequency responses of the magnitude of shear modulus and the loss angle for the Etna 1992 top sample at 786 °C (*James et al., 2004*).

f [Hz]	$|G^*|$ [GPa]	loss angle [rad]
0.002	7.8984	0.029311
0.005	8.6888	0.02522
0.01	9.6538	0.023243
0.02	10.968	0.019216
0.05	11.665	0.016594
0.1	12.721	0.013335
0.2	15.352	0.0120599
0.5	17.345	0.01170799
1	18.169	0.0102132
2	19.268	0.0088959
5	20.627	0.0064447
10	21.312	0.0046908
20	21.669	0.0039605

132